

Persistence of Island Arrangements During Layer-by-Layer Growth Revealed Using Coherent X-rays

Guangxu Ju,¹ Dongwei Xu,^{1,*} Matthew J. Highland,¹ Carol Thompson,² Hua Zhou,³ Jeffrey A. Eastman,¹ Paul H. Fuoss,^{1,†} Peter Zapol,¹ Hyunjung Kim,⁴ and G. Brian Stephenson^{1,‡}

¹*Materials Science Division, Argonne National Laboratory, Argonne, IL 60439 USA*

²*Department of Physics, Northern Illinois University, DeKalb IL 60115 USA*

³*X-ray Science Division, Argonne National Laboratory, Argonne, IL 60439 USA*

⁴*Department of Physics, Sogang University, Seoul, 04107 Korea*

(Dated: April 22, 2018)

Understanding surface dynamics during epitaxial film growth is key to growing high quality materials with controllable properties. X-ray photon correlation spectroscopy (XPCS) using coherent x-rays opens new opportunities for *in situ* observation of atomic-scale fluctuation dynamics during crystal growth. Here, we present the first XPCS measurements of 2D island dynamics during homoepitaxial growth in the layer-by-layer mode. Analysis of the results using two-time correlations reveals a new phenomenon – a memory effect in island nucleation sites on successive crystal layers. Simulations indicate that this persistence in the island arrangements arises from communication between islands on different layers via adatoms. With the worldwide advent of new coherent x-ray sources, the XPCS methods pioneered here will be widely applicable to atomic-scale processes on surfaces.

Nanoscale structures generated by growth processes during phase transitions are ubiquitous in synthesis of advanced materials, and are often central to their outstanding properties. These include systems as diverse as precipitates and twin textures in high strength and shape-memory alloys¹⁻³, spatio-temporal patterns in surface reconstructions and nanoparticles driven by catalytic chemistry^{4,5}, and domain patterns in ferroic thin films that generate high dielectric, conductivity, piezoelectric, and magnetic responses^{6,7}. To understand the competing fundamental processes that control nucleation and growth of these structures, we need to observe more than just the average nucleation rate or density, but also the preferred sites and arrangements. X-ray scattering methods are well suited for directly observing the formation of such structures *in situ* during materials synthesis, although traditional methods with incoherent x-rays typically provide only spatially averaged quantities. The advent of coherent x-ray methods has opened a new window into phase transition mechanisms, by revealing the dynamics of the exact nanostructure arrangement and its fluctuations⁸.

Standard x-ray photon correlation spectroscopy (XPCS) analysis characterizes the time correlation of fluctuations in equilibrium or steady-state systems. In many cases, the correlations simply decay exponentially, and the wavenumber (Q) dependence of the correlation time provides direct information about the mechanism of the fluctuation dynamics⁹⁻¹². In other cases, heterodyne mixing between scattering from different regions produces oscillatory correlations, allowing the relative velocities of different structural features to be determined¹³.

When the average structure is not constant in time, e.g. during domain nucleation and growth¹⁴⁻¹⁹, coarsening²⁰⁻²³, or structural relaxation^{24,25}, a two-time XPCS analysis can be applied²⁶. For domain coarsening processes, such analysis has shown that the domain arrangement can be remarkably independent of time, with the random pattern es-

established by the initial nucleation process simply amplified or diminished at different Q by coarsening^{20,22,27,28}. Nucleation of magnetic domains during field cycling has been shown to exhibit a memory effect^{14,16-19}, with strong correlations between the domain arrangements occurring on each cycle of the field.

Here we explore the spatio-temporal correlations of two-dimensional (2D) nanostructures produced in a different class of phase transition - crystal growth from the vapor. During crystal growth in the layer-by-layer growth mode, deposited atoms diffuse on the surface to nucleate islands of single monolayer (ML) height, which grow and coalesce to form a complete layer^{29,30}. This process of 2D island nucleation and coalescence repeats in a cyclic fashion to form each layer of the crystal. Current models predict that the arrangement of islands reflects a competition between nucleation of new islands versus attachment to existing islands, kinetically controlled by the relative rates of deposition and adatom diffusion, and affected by the Ehrlich-Schwoebel (ES) barrier for diffusion over step edges³¹. To investigate these fundamental phenomena, we have chosen to study metal-organic vapor phase epitaxy (MOVPE) of GaN on its (10 $\bar{1}$ 0) m-plane surface, a growth orientation of interest for advanced solid-state lighting and high power electronics³². Previous *in situ* x-ray scattering studies with incoherent x-rays³³ have characterized the layer-by-layer growth mode in this system, and mapped the average island spacing and shape. Using XPCS, we have discovered that the island arrangements on each layer can be highly correlated, persisting over several monolayers of growth. To understand the cause of this persistence, we have performed kinetic Monte Carlo (KMC) simulations of the growth process. These show a similar persistence in the island arrangements between layers, indicating that the effect is not due to nucleation at fixed defects as in magnetic domain systems¹⁹, but is instead due to communication from layer to layer via the adatom density distribution.

XPCS MEASUREMENTS

Because of the low scattering cross section of 2D islands, developing XPCS methods to study their dynamics presents significant challenges. To date, XPCS studies of atomic-height surface features have been performed only on strongly scattering systems such as Au with relatively large ($\sim 1 \mu\text{m}$) in-plane structures^{9,34}. The higher x-ray energy ($E \approx 25 \text{ keV}$) required for *in situ* studies, to penetrate the environment and to avoid interaction of the x-ray beam with the growth process, creates an additional challenge since both the coherent x-ray flux available from the source and the solid angle required to resolve speckle at the detector scale as E^{-2} . To increase the transversely coherent flux available from the source, we removed the monochromator and accepted the full pink beam bandwidth ($\Delta E/E = 1.3 \times 10^{-2}$) of the third harmonic of the undulator spectrum. While this relatively large bandwidth decreases the Q resolution in the radial direction, it can be adequate for near-specular XPCS measurements from surface features, since the speckle are extended in the surface normal direction (Supplementary Fig. 4). A special x-ray optical setup was developed to optimize the coherence lengths and remove unwanted harmonics from the undulator spectrum (Fig. 1(a) and Supplementary Section 1). We also developed correlation analysis techniques optimized for low signals.

Another major challenge in performing an *in situ* XPCS study of growth is to maintain position and angular stability of the sample at high temperature so that the incident beam illuminates the same area during the growth process. We developed a special chamber and instrument for coherent x-ray studies during *in situ* growth by MOVPE³⁵, and verified that

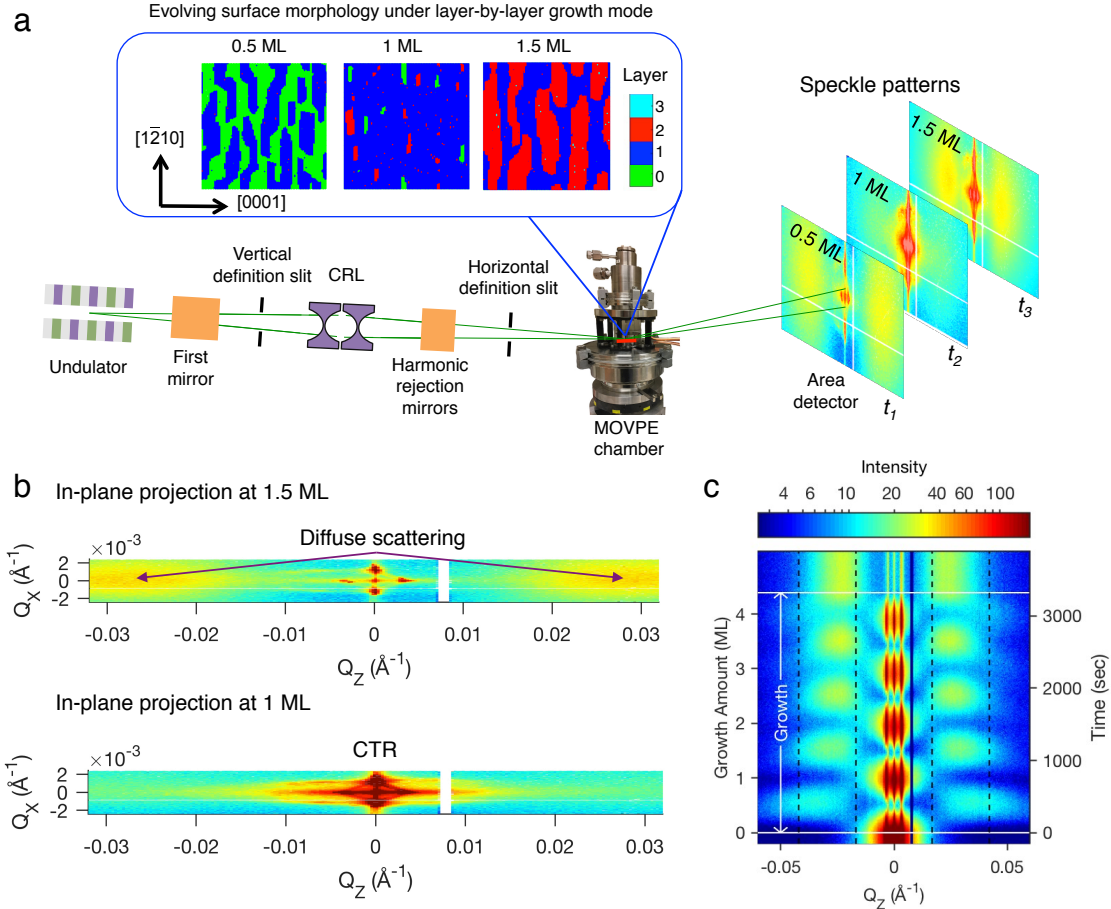


FIG. 1. Experimental schematic and diffuse scattering from islands. **a**, The evolving arrangement of atomic-height islands during metal-organic vapor phase epitaxy (MOVPE) on the GaN $(10\bar{1}0)$ m-plane surface is recorded as a function of time in the speckle pattern produced by a partially coherent x-ray beam prepared by a special optical setup (Supplementary Section 1). **b**, Scattering patterns recorded near the $Q_Y = 1.09 \text{ \AA}^{-1}$ position along the specular direction are projected onto the Q_X - Q_Z surface plane in reciprocal space, so that features can be directly related to the surface morphology. (White lines near $Q_Z = 0.008$ and $Q_X = -0.001 \text{ \AA}^{-1}$ are artifacts from the missing pixels between the detector quadrants.) In the typical images shown, diffuse scattering at $Q_Z \approx 0.025 \text{ \AA}^{-1}$ arises from 2D islands with spacings of $\sim 25 \text{ nm}$, while crystal truncation rods (CTRs) at low Q_Z arise from $\sim 10 \mu\text{m}$ facets having $\sim 100 \text{ nm}$ atomic terraces (Supplementary Fig. 1 and Section 2). Speckle in the diffuse scattering allows analysis of the spatio-temporal correlations in the island arrangement. **c**, Intensity integrated between $Q_X = \pm 3 \times 10^{-4} \text{ \AA}^{-1}$ as a function of time during growth of 4.5 monolayers (1 ML = 0.276 nm) in the layer-by-layer mode at 796 K. Times of growth start and end are indicated. During growth, the CTR intensity oscillates with time, with minima and maxima at half- and full-integer-ML amounts of growth, respectively, owing to destructive interference between scattering by each successive layer at this Q_Y . The diffuse scattering intensity oscillates out of phase with the CTRs, with maxima at half-integer ML when island density is largest, and minima at full-integer ML when islands have coalesced to form a new layer.

it had the required stability (Supplementary Fig. 5 and Section 3).

During homoepitaxial growth of GaN on the $(10\bar{1}0)$ m-plane surface, the islands that form are elongated perpendicular to the $[0001]$ direction because of step edge energy anisotropy^{33,36}. This concentrates the diffuse scattering into the Q_Z direction (Fig. 1(b)). We monitored the speckle pattern in the diffuse scattering from islands near the specular rod $(H0\bar{H}0)$ at $H = 0.48$, close to but just off the anti-Bragg position because of the residual harmonic contamination at $H = 0.5$. The intensity of the diffuse scattering from the islands oscillates out of phase with the crystal truncation rod (CTR) intensity (Fig. 1(c)), as expected for layer-by-layer growth³³. A slow growth rate of $\sim 1.3 \times 10^{-3}$ ML/s was used to increase signal collection time, and temperatures studied were chosen to span across the layer-by-layer growth regime³³.

Because the system is not at steady-state during layer-by-layer growth and the average intensity is oscillating with time, we analyzed the speckle pattern sequence using a two-time correlation function for wavevector \mathbf{Q} and times t_1 and t_2 ,

$$C(t_1, t_2) = \left\langle \frac{\Delta I(\mathbf{Q}, t_1) \Delta I(\mathbf{Q}, t_2)}{\bar{I}(\mathbf{Q}, t_1) \bar{I}(\mathbf{Q}, t_2)} \right\rangle_{\mathbf{Q}}, \quad (1)$$

where $\Delta I(\mathbf{Q}, t_i) \equiv I(\mathbf{Q}, t_i) - \bar{I}(\mathbf{Q}, t_i)$ is the deviation of the intensity in the speckle pattern from the mean intensity \bar{I} that would be measured under incoherent conditions where the speckles are not resolved. For analysis of our experimental results, where the mean intensity \bar{I} varies with time, we obtain $\bar{I}(\mathbf{Q}, t)$ by smoothing $I(\mathbf{Q}, t)$ over a range of neighboring detector pixels, and we obtain the ensemble average $\langle \rangle$ by averaging over a range of \mathbf{Q} having similar time correlations (Supplementary Table 1 and Section 3). This form of the two-time correlation function gives values which are analogous to the contrast of a distribution, since the diagonal elements with $t_1 = t_2$ are equal to the observed variance divided by the square of the mean. The measured speckle contrast values are in good agreement with those expected from the properties of the x-ray illumination and the detector (Supplementary Figs. 2, 3). Values of C greater than, equal to, or less than zero correspond to island arrangements which are correlated, uncorrelated, and anti-correlated, respectively.

To characterize the 2D island arrangements, we extract two-time correlations in the diffuse scattering (Fig. 2(a)). The ‘‘checkerboard’’ pattern evident in the two-time correlations during growth reveals a surprising result – even though the island arrangement is determined by a statistical nucleation process to form each atomic layer of the crystal, the arrangement is correlated across several successive layers, indicating a memory effect in the nucleation locations. This is similar to the return point memory effect found in magnetic thin films^{14,16–19}, in which the same pattern of domains can form again after being erased during field cycling. These changing correlations are clearly produced by the growth process, since the two-time correlations for the periods before and after growth indicate that the island arrangement remains fixed.

KMC SIMULATIONS

As a comparison to the XPCS experiments, we carried out simulations of layer-by-layer growth on an m-plane GaN surface and calculated the two-time correlations in the simulated diffuse scattering. Because the simulations are free of crystal defects, this allows us to investigate whether persistence in the island arrangement is intrinsic to the layer-by-layer growth process, or is instead produced by preferred nucleation at fixed defects (as is

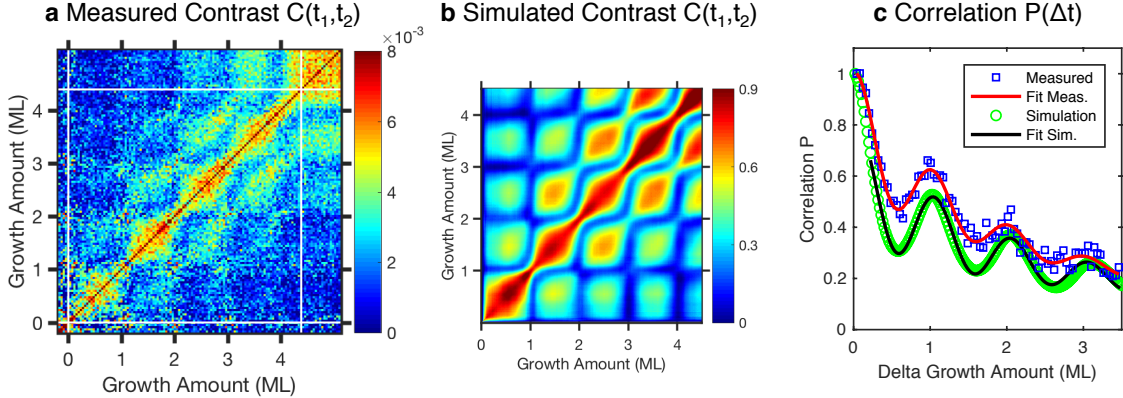


FIG. 2. **Oscillating correlations.** **a**, Two-time correlations in the measured speckle from 2D islands before, during, and after growth at 796 K. The time axes have been converted to growth amount using the observed growth rate (Supplementary Table 2). White lines indicate the start and end of growth. The “checkerboard” pattern indicates that the arrangement of islands formed in successive layers is correlated with that in previous layers. **b**, Two-time correlations in the simulated speckle from 2D islands during growth, which also show correlations between island arrangements in successive layers. **c**, Points: measured and simulated correlations averaged over equal time differences, showing oscillatory behavior with a period of 1 ML. Curves: fits to equation (3).

found for magnetic domains^{19,37}). The KMC model used has been found to reproduce the phenomenology of MOVPE growth on m-plane GaN³⁶. While the simulation is necessarily carried out on a smaller system than the experiments, the temperature and growth rate in the simulation were chosen to give a similar number of islands per terrace (~ 5) as in the experiments (Supplementary Section 4). Figure 2(b) shows the simulated two-time correlations. (For the simulations, the mean intensity \bar{I} in equation (1) is calculated by averaging over 16 random initial conditions, rather than by smoothing in \mathbf{Q} .) These show a strong checkerboard pattern from persistence of the island arrangement from layer to layer, even in the absence of crystal defects. To understand the meaning of the statistical analysis, it is helpful to examine images of the 2D islands and steps from the simulations after different amounts of growth (Fig. 3). One can see that the island arrangement at 2.5 ML has many features in common with that at 1.5 ML. For example, the yellow regions on the right half of the 2.5 ML image are similar to the blue regions on the right half of the 1.5 ML image.

ISLAND ARRANGEMENT PERSISTENCE

To quantify the island arrangement persistence, we define the quantity P by averaging the two-time correlation over lines running parallel with the main diagonal, representing equal time differences Δt perpendicular to the diagonal,

$$P(\Delta t) = \frac{\langle C(t, t + \Delta t) \rangle_t}{\langle C(t, t + \delta) \rangle_t}. \quad (2)$$

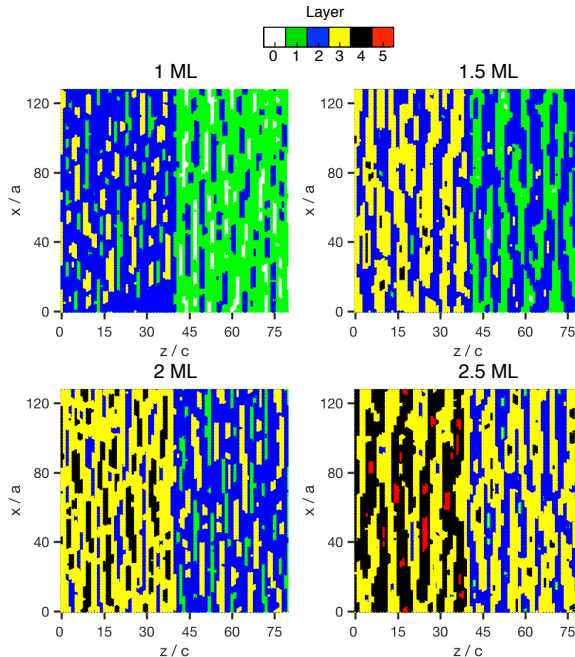


FIG. 3. **Correlations of island positions.** Kinetic Monte Carlo simulations of surface island and step arrangements after 1.0, 1.5, 2.0, and 2.5 ML of layer-by-layer growth on m-plane GaN, for one of the 16 random initial conditions used. Colors indicate the surface height, and positions x or z are specified in terms of the number of a or c lattice parameters in the $[1\bar{2}10]$ or $[0001]$ directions, respectively. The vicinal surface has an initial step spacing producing terraces half the z width of the simulation. Monolayer-height islands nucleate and coalesce on the terraces to form each layer during growth, and their arrangement is correlated from layer to layer.

The numerator is equal to the standard intensity autocorrelation function $g_2 - 1$ ³⁸. We have normalized P to the value at the minimum non-zero $\Delta t \equiv \delta$, leaving out the point at $\Delta t = 0$ because it contains self-correlated shot noise (Supplementary Section 3). Both the measured and simulated P values exhibit decaying oscillations (Figs. 2(c) and (d)), with peaks near integer ML positions, indicating a tendency for the island arrangement at any time to repeat after one or more integer monolayers for growth. In order to extract the main features from this behavior, we have fit $P(\Delta t)$ to the empirical form

$$P(\Delta t) = P_0 + A_0 \exp(-\Delta t/\tau_0) + A^* \exp(-\Delta t/\tau^*) \cos(2\pi(\Delta t + \Delta t_0)), \quad (3)$$

where the 2nd and 3rd terms represent average and oscillating components that decay with time constants τ_0 and τ^* , respectively. For display, we have converted the time differences Δt and corresponding fit parameters to ML of growth. This empirical form adequately captures the decay of the oscillations of $P(\Delta t)$ in the measurements, and in the simulations beginning at the first 0.2 ML of growth.

Similar oscillating g_2 functions have been observed recently in grazing-incidence small-angle x-ray scattering from surface roughness during sputter deposition of amorphous films¹³. In that study, the oscillations arise from heterodyne interference between scattering from the surface and from defects in the bulk of the film, and the period of the heterodyne oscillations is inversely related to the product of the wavevector and the velocity vector of

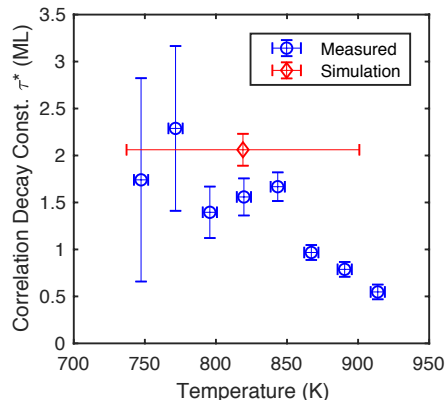


FIG. 4. **Persistence times of island arrangements.** Decay constant τ^* of the oscillatory part of the correlation functions shown in Fig. 2 as function of growth temperature. Measured correlations persist for about 2 ML of growth up to 850 K, in agreement with the simulation.

the advancing surface. In our case, the heterodyne period would be $H^{-1} \approx 2.08$ ML per oscillation at our relatively high wavenumber of $H \approx 0.48$ r.l.u. We instead see a period of 1 ML per oscillation, equal to the period of the island nucleation and coalescence during layer-by-layer growth. Thus we are observing homodyne oscillations arising from correlations between island arrangements on subsequent layers, rather than heterodyne effects from the surface velocity.

We performed the same two-time analysis for eight experimental datasets obtained at growth temperatures T spanning the range across the layer-by-layer growth regime, at fixed growth rate (Supplementary Figs. 6, 7 and Table 2). The decay constant τ^* of the oscillatory part of $P(\Delta t)$ shows a systematic dependence on T (Fig. 4), with a value of about 2 ML at lower T , decreasing at higher T as the transition to step-flow growth at $T \approx 930$ K is approached. The value of τ^* obtained from the simulations agrees reasonably well with the experiments, although correspondence between the simulation and experimental temperatures is uncertain (Supplementary Section 4).

Based on the physics underlying island nucleation, we propose the following mechanism for the observed island arrangement persistence in layer-by-layer growth. As one layer completes, nucleation events for 2D islands in the next layer preferentially occur in regions of high adatom density. The adatom density distribution is affected by the location of island and step edges in the almost-complete layer. Analysis of step-flow growth indicates that adatom distributions above a step edge depend upon the magnitude of the ES barrier³¹, and the same phenomenon will affect adatom distributions on top of existing islands during layer-by-layer growth. When the ES barrier is low, the island edges act as sinks for adatoms, so the maximum adatom density will be in the center of the islands (Fig. 5). This will favor nucleation of islands in the next layer to occur near the nucleation locations of the previous layer, leading to persistent island arrangements. If the ES barrier has a medium value, the edges are less effective sinks, the adatom density and nucleation locations are more uniform, and the persistence will be lower. A high ES barrier will inhibit island coalescence, changing the growth mode from layer-by-layer to 3D. Thus island arrangement persistence revealed by XPCS provides a sensitive new probe of interlayer transport during crystal growth.

In summary, we have performed the first XPCS measurements of 2D island dynamics during layer by layer growth. The experiments demonstrate that the full bandwidth of an

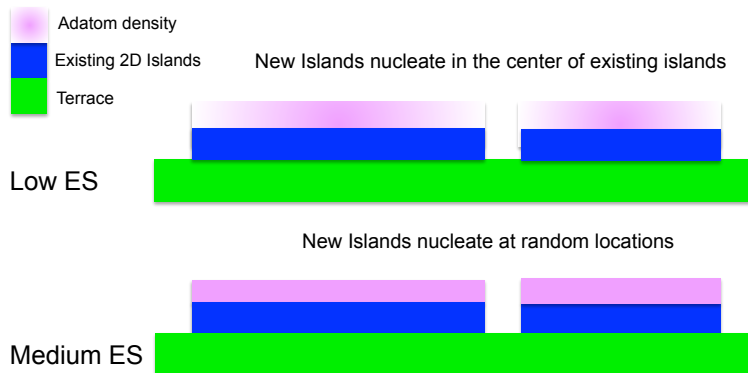


FIG. 5. **Mechanism for island arrangement persistence.** Schematic atomic-scale cross sections during layer-by-layer growth, showing dilute adatom density (pink) on tops of existing 2D islands just before they coalesce (blue), for systems with low and medium Ehrlich-Schwoebel (ES) barriers. For low ES barriers, the island edges act as a sink for adatoms, so their density (and thus the nucleation rate of islands in the next layer) is maximum in the center of islands. For medium ES barriers, adatom densities are more uniform, leading to more random nucleation locations. High ES barriers (not shown) produce 3D growth.

undulator harmonic can be used for XPCS studies of atomic-scale surface dynamics, making it possible to obtain sufficient signal to measure two-time correlations in the diffuse scattering from monolayer-height islands. The observed correlations show a new phenomenon, persistent 2D island arrangements during layer-by-layer growth. The phenomenon is also observed in kinetic Monte Carlo simulations of layer-by-layer growth, indicating that it arises by communication of the arrangement of islands in the underlying layer to those in the newly forming layer via the adatom density distribution. The XPCS results provide new ways to test models of crystal growth and to understand the atomic scale phenomena that allow us to control and optimize materials synthesis processes. For example, atomic step patterns on substrate surfaces can directly control the domain patterns in deposited epitaxial layers^{39,40}.

The two-time correlations discussed here are but one of many higher-order correlation functions that can be explored by coherent x-ray methods^{8,41}, providing a richer view of the atomic-scale processes that give rise to ordered nanostructures. The penetrating nature of high energy x-rays will allow these studies in native operating environments critical to applications. The methods developed here for the model GaN MOVPE growth system open the way for studies of surface dynamics in many other areas, such as growth of bulk crystals or quasi-two-dimensional materials in reactive sputtering or pulsed laser deposition, or from the liquid phase. The greatly enhanced coherence of x-ray beams soon to be provided by new and upgraded hard x-ray sources⁴² will produce speckle in the scattering from every system, enabling XPCS studies across broad areas of physics.

METHODS

The experiments were carried out at beamline 12ID-D at the Advanced Photon Source (APS), using a goniometer and MOVPE system specifically developed for coherent x-ray

studies³⁵. An intense “pink beam” with appropriate coherence characteristics was prepared using a setup similar to that described previously⁴³, with the addition of a harmonic rejection mirror pair (Supplementary Section 1). The beam incident on the sample had a typical intensity of 1.4×10^{12} photons per second at $E = 25.75$ keV, in a spot size of $4 \times 16 \mu\text{m}$ with transverse coherence lengths of $1.2 \times 2.7 \mu\text{m}$ in the vertical and horizontal, respectively. X-ray speckle patterns were recorded using a photon counting area detector with a GaAs sensor having 512×512 pixels, $55 \mu\text{m}$ pixel size, located 2.39 m from the sample (Amsterdam Scientific Instruments LynX 1800). Data were corrected for the measured flat-field response of the detector. Dynamics were recorded with a sequence of 10 s integrations, subsequently binned by 3 in time.

MOVPE growth of GaN on the m-plane surface was carried out using procedures and substrates described previously³³. Substrate temperatures were calibrated to within ± 5 K³⁵. Growth was started or stopped by injecting or venting a supply of the Ga precursor triethylgallium (TEGa), with a large oversupply of the N precursor (NH_3) constantly supplied. Growth runs were performed at eight different temperatures using the same TEGa flow ($4.0 \times 10^{-3} \mu\text{mole}/\text{min}$). The same substrate was used for all growths; it was annealed for 300 s at $T = 1120$ K between growths to recover the same initial surface condition with minimal islands. To account for thermal expansion of the heater, the position of the sample was realigned between growths, so slightly different regions of the surface were investigated at each temperature. Growth rates were extracted from the oscillation periods of the diffuse and CTR scattering. They varied by about 10% from growth to growth around a mean of 1.25×10^{-3} ML/s (Supplementary Table 2). The growth rate was constant during a given growth, apart from a $\sim 5\%$ lower growth rate for the first ML.

Calculated two-time correlations in the scattering from islands were derived from KMC simulations on the m-plane surface of a three-dimensional HCP lattice³⁶. The dynamics of deposition and diffusion on a stepped surface were simulated using a variable time step method as implemented in the Stochastic Parallel Particle Kinetic Simulator (SPPARKS) computer code⁴⁴ (Supplementary Section 4).

Raw x-ray data were generated at the Advanced Photon Source large-scale facility. Derived data and simulations supporting the findings of this study are available from the corresponding author upon request.

* current address: School of Energy and Power Engineering, Huazhong University of Science and Technology, Wuhan 430074, China

† current address: SLAC National Accelerator Laboratory, Menlo Park, CA 94025 USA

‡ correspondence to: stephenson@anl.gov

¹ Yintao Song, Xian Chen, Vivekanand Dabade, Thomas W. Shield, and Richard D. James, “Enhanced reversibility and unusual microstructure of a phase-transforming material,” *Nature* **502**, 85–88 (2013).

² Yukiko Ogawa, Daisuke Ando, Yuji Sutou, and Junichi Koike, “A lightweight shape-memory magnesium alloy,” *Science* **353**, 368–370 (2016), <http://science.sciencemag.org/content/353/6297/368.full.pdf>.

³ Yu. N. Gornostyrev and M. I. Katsnelson, “Misfit stabilized embedded nanoparticles in metallic alloys,” *Physical Chemistry Chemical Physics* **17**, 27249–27257 (2015).

⁴ Alexander S. Mikhailov and Kenneth Showalter, “Control of waves, patterns and turbulence in

- chemical systems,” *Physics Reports* **425**, 79–194 (2006).
- ⁵ Fan Jiang, A. Munkholm, R. V Wang, S. K. Streiffer, Carol Thompson, P. H. Fuoss, K. Latifi, K. R. Elder, and G. B. Stephenson, “Spontaneous oscillations and waves during chemical vapor deposition of InN,” *Physical Review Letters* **101**, 086102 (2008).
 - ⁶ A. S. McLeod, E. van Heumen, J. G. Ramirez, S. Wang, T. Saerbeck, S. Guenon, M. Goldflam, L. Anderegg, P. Kelly, A. Mueller, M. K. Liu, Ivan K. Schuller, and D. N. Basov, “Nanotextured phase coexistence in the correlated insulator V_2O_3 ,” *Nature Physics* **13**, 80–86 (2016).
 - ⁷ Fei-Ting Huang and Sang-Wook Cheong, “Aperiodic topological order in the domain configurations of functional materials,” *Nature Reviews Materials* **2**, 17004 (2017).
 - ⁸ Oleg G. Shpyrko, “X-ray photon correlation spectroscopy,” *Journal of Synchrotron Radiation* **21**, 1057–1064 (2014).
 - ⁹ M. S. Pierce, K. C. Chang, D. Hennessy, V. Komanicky, M. Sprung, A. Sandy, and H. You, “Surface x-ray speckles: coherent surface diffraction from Au (001),” *Physical Review Letters* **103**, 165501 (2009).
 - ¹⁰ Hyunjung Kim, A. Rühm, L. B. Lurio, J. K. Basu, J. Lal, D. Lumma, S. G. J. Mochrie, and S. K. Sinha, “Surface dynamics of polymer films,” *Physical Review Letters* **90**, 068302 (2003).
 - ¹¹ B. Ruta, G. Baldi, Y. Chushkin, Benoit Rufflé, L. Cristofolini, Adriano Fontana, M. Zanatta, and Francesco Nazzani, “Revealing the fast atomic motion of network glasses,” *Nature Communications* **5**, 3939 (2014).
 - ¹² W. Roseker, S. O. Hruszkewycz, F. Lehmkuhler, M. Walther, H. Schulte-Schrepping, S. Lee, T. Osaka, L. Strüder, R. Hartmann, M. Sikorski, S. Song, A. Robert, P. H. Fuoss, M. Sutton, G. B. Stephenson, and G. Grübel, “Towards ultrafast dynamics with split-pulse x-ray photon correlation spectroscopy at free electron laser sources,” *Nature Communications* (2018), in press.
 - ¹³ Jeffrey G. Ulbrandt, Meliha G. Rainville, Christa Wagenbach, Suresh Narayanan, Alec R. Sandy, Hua Zhou, Karl F. Ludwig Jr., and Randall L. Headrick, “Direct measurement of the propagation velocity of defects using coherent x-rays,” *Nature Physics* **12**, 794–799 (2016).
 - ¹⁴ Michael S. Pierce, Rob G. Moore, Larry B. Sorensen, Stephen D. Kevan, Olav Hellwig, Eric E. Fullerton, and Jeffrey B. Kortright, “Quasistatic x-ray speckle metrology of microscopic magnetic return-point memory,” *Physical Review Letters* **90**, 175502 (2003).
 - ¹⁵ Christopher Sanborn, Karl F. Ludwig, Michael C. Rogers, and Mark Sutton, “Direct measurement of microstructural avalanches during the martensitic transition of cobalt using coherent x-ray scattering,” *Physical Review Letters* **107**, 015702 (2011).
 - ¹⁶ Karine Chesnel, Joseph A. Nelson, Stephen D. Kevan, Matthew J. Carey, and Eric E. Fullerton, “Oscillating spatial dependence of domain memory in ferromagnetic films mapped via x-ray speckle correlation,” *Physical Review B* **83**, 054436 (2011).
 - ¹⁷ Karine Chesnel, Brian Wilcken, Matthew Rytting, Steve D. Kevan, and Eric E. Fullerton, “Field mapping and temperature dependence of magnetic domain memory induced by exchange couplings,” *New Journal of Physics* **15**, 023016 (2013).
 - ¹⁸ Karine Chesnel, Alex Safsten, Matthew Rytting, and Eric E. Fullerton, “Shaping nanoscale magnetic domain memory in exchange-coupled ferromagnets by field cooling,” *Nature Communications* **7**, 11648 (2016).
 - ¹⁹ M. S. Pierce, C. R. Buechler, L. B. Sorensen, J. J. Turner, S. D. Kevan, E. A. Jagla, J. M. Deutsch, T. Mai, O. Narayan, J. E. Davies, K. Liu, J. Hunter Dunn, K. M. Chesnel, J. B. Kortright, O. Hellwig, and E. E. Fullerton., “Disorder-induced microscopic magnetic memory,” *Physical Review Letters* **94**, 017202 (2005).

- ²⁰ A. Malik, A. R. Sandy, L. B. Lurio, G. B. Stephenson, S. G. J. Mochrie, I. McNulty, and M. Sutton, “Coherent x-ray study of fluctuations during domain coarsening,” [Physical Review Letters](#) **81**, 5832–5835 (1998).
- ²¹ F. Livet, F. Bley, R. Caudron, E. Geissler, D. Abernathy, C. Detlefs, G. Grübel, and M. Sutton, “Kinetic evolution of unmixing in an AlLi alloy using x-ray intensity fluctuation spectroscopy,” [Physical Review E](#) **63**, 036108 (2001).
- ²² Andrei Fluerasu, Mark Sutton, and Eric M. Dufresne, “X-ray intensity fluctuation spectroscopy studies on phase-ordering systems,” [Physical Review Letters](#) **94**, 055501 (2005).
- ²³ Young Yong Kim, Kyungtae Kim, Sungmin Jung, Changsub Kim, Jehan Kim, Stephan V Roth, Michael Sprung, Ivan A. Vartanyants, and Moonhor Ree, “Synchrotron x-ray scattering and photon correlation spectroscopy studies on thin film morphology details and structural changes of an amorphous-crystalline brush diblock copolymer,” [Polymer](#) **105**, 472–486 (2016).
- ²⁴ X. D. Wang, B. Ruta, L. H. Xiong, D. W. Zhang, Y. Chushkin, H. W. Sheng, H. B. Lou, Q. P. Cao, and J. Z. Jiang, “Free-volume dependent atomic dynamics in beta relaxation pronounced La-based metallic glasses,” [Acta Materialia](#) **99**, 290–296 (2015).
- ²⁵ Beatrice Ruta, Federico Zontone, Yuriy Chushkin, Giacomo Baldi, Giovanna Pintori, Giulio Monaco, Benoit Rufflé, and Walter Kob, “Hard x-rays as pump and probe of atomic motion in oxide glasses,” [Scientific Reports](#) **7**, 3962 (2017).
- ²⁶ Oier Bikondoa, “On the use of two-time correlation functions for x-ray photon correlation spectroscopy data analysis,” [Journal of Applied Crystallography](#) **50**, 357–368 (2017).
- ²⁷ Gregory Brown, Per Arne Rikvold, Mark Sutton, and Martin Grant, “Speckle from phase-ordering systems,” [Physical Review E](#) **56**, 6601 (1997).
- ²⁸ Gregory Brown, Per Arne Rikvold, Mark Sutton, and Martin Grant, “Evolution of speckle during spinodal decomposition,” [Physical Review E](#) **60**, 5151–5162 (1999).
- ²⁹ J. H. Neave, B. A. Joyce, P. J. Dobson, and N. Norton, “Dynamics of film growth of GaAs by MBE from RHEED observations,” [Applied Physics A](#) **31**, 1–8 (1983).
- ³⁰ Jeffrey Y. Tsao, *Materials fundamentals of molecular beam epitaxy* (Academic Press, 1993).
- ³¹ Nils A. K. Kaufmann, L. Lahourcade, B. Hourahine, D. Martin, and N. Grandjean, “Critical impact of Ehrlich–Schwöbel barrier on GaN surface morphology during homoepitaxial growth,” [Journal of Crystal Growth](#) **433**, 36–42 (2016).
- ³² Steven P. DenBaars, Daniel Feezell, Katheryn Kelchner, Siddha Pimputkar, Chi-Chen Pan, Chia-Chen Yen, Shinichi Tanaka, Yuji Zhao, Nathan Pfaff, Robert Farrell, Mike Iza, Stacia Keller, Umesh Mishra, James S. Speck, and Shuji Nakamura, “Development of gallium-nitride-based light-emitting diodes (LEDs) and laser diodes for energy-efficient lighting and displays,” [Acta Materialia](#) **61**, 945–951 (2013).
- ³³ Edith Perret, Dongwei Xu, M. J. Highland, G. B. Stephenson, P. Zapol, P. H. Fuoss, A. Munkholm, and Carol Thompson, “Island dynamics and anisotropy during vapor phase epitaxy of m-plane GaN,” [Applied Physics Letters](#) **111**, 232102 (2017).
- ³⁴ Michael S. Pierce, Vladimir Komanicky, Andi Barbour, Daniel C. Hennessy, Chenhui Zhu, Alec Sandy, and Hoydoo You, “Dynamics of the Au (001) surface in electrolytes: in situ coherent x-ray scattering,” [Physical Review B](#) **86**, 085410 (2012).
- ³⁵ Guangxu Ju, Matthew J. Highland, Angel Yanguas-Gil, Carol Thompson, Jeffrey A. Eastman, Hua Zhou, Sean M. Brennan, G. Brian Stephenson, and Paul H. Fuoss, “An instrument for in situ coherent x-ray studies of metal-organic vapor phase epitaxy of III-nitrides,” [Review of Scientific Instruments](#) **88**, 035113 (2017).
- ³⁶ Dongwei Xu, Peter Zapol, G. Brian Stephenson, and Carol Thompson, “Kinetic Monte Carlo

- simulations of GaN homoepitaxy on c-and m-plane surfaces,” *The Journal of Chemical Physics* **146**, 144702 (2017).
- ³⁷ Laura Martín-García, Gong Chen, Yaiza Montaña, Arantzazu Mascaraque, Beatriz M. Pabón, Andreas K. Schmid, and Juan de la Figuera, “Memory effect and magnetocrystalline anisotropy impact on the surface magnetic domains of magnetite(001),” *Scientific Reports* **8**, 5991 (2018).
- ³⁸ Sunil K. Sinha, Zhang Jiang, and Laurence B. Lurio, “X-ray photon correlation spectroscopy studies of surfaces and thin films,” *Advanced Materials* **26**, 7764–7785 (2014).
- ³⁹ Carol Thompson, D. D. Fong, R. V. Wang, F. Jiang, S. K. Streiffer, K. Latifi, J. A. Eastman, P. H. Fuoss, , and G. B. Stephenson, “Imaging and alignment of nanoscale 180° stripe domains in ferroelectric thin films,” *Applied Physics Letters* **93**, 182901 (2008).
- ⁴⁰ G. Mattoni, P. Zubko, F. Maccherozzi, A. J. H. van der Torren, D. B. Boltje, M. Hadjimichael, N. Manca, S. Catalano, M. Gibert, Y. Liu, J. Aarts, J.-M. Triscone, S. S. Dhesi, and A. D. Caviglia, “Striped nanoscale phase separation at the metal-insulator transition of heteroepitaxial nickelates,” *Nature Communications* **7**, 13141 (2016).
- ⁴¹ Sylvain Ravy, “Homometry in the light of coherent beams,” *Acta Crystallographica Section A: Foundations of Crystallography* **69**, 543–548 (2013).
- ⁴² Robert Hettel, “DLSR design and plans: an international overview,” *Journal of Synchrotron Radiation* **21**, 843–855 (2014).
- ⁴³ Guangxu Ju, Matthew J. Highland, Carol Thompson, Jeffrey A. Eastman, Paul H. Fuoss, Hua Zhou, Roger Dejus, and G. Brian Stephenson, “Characterization of the x-ray coherence properties of an undulator beamline at the Advanced Photon Source,” *Preprint at <https://arxiv.org/abs/1802.05675>* (2018).
- ⁴⁴ Steve Plimpton, Corbet Battaile, Mike Chandross, Liz Holm, Aidan Thompson, Veena Tikare, Ed Wagner, Greg and Webb, Xiaowang Zhou, Cristina Garcia Cardona, and Alex Slepoy, *Crossing the Mesoscale No-Man’s Land via Parallel Kinetic Monte Carlo*, Tech. Rep. SAND2009–6226 (Sandia National Laboratories, 2009).

ACKNOWLEDGMENTS

We thank Mark Sutton for suggesting the smoothing method used in the speckle analysis, and Dmitry Byelov of ASI and Russell Woods of the APS Detector Pool for expert assistance with the area detector. Support provided by the Department of Energy, Office of Science, Basic Energy Sciences, Materials Sciences and Engineering (XPCS measurements and analysis) and Scientific User Facilities (KMC model development). Measurements were carried out at the Advanced Photon Source, a DOE Office of Science user facility operated by Argonne National Laboratory. Computing resources were provided on Blues and Fusion, high-performance computing clusters operated by the Laboratory Computing Resource Center at Argonne National Laboratory.

AUTHOR CONTRIBUTIONS

G.J., M.J.H., J.A.E, P.H.F., G.B.S., C.T., H.Z., and H.K. developed the pink beam XPCS setup and carried out the measurements. D.X., P.Z., G.B.S., and C.T. developed and carried out the simulations. G.J. and G.B.S. analyzed the results. All coauthors contributed to drafting and editing the manuscript.

ADDITIONAL INFORMATION

Supplementary Information accompanies this paper. Correspondence and requests for materials or data should be addressed to G.B.S.